RSC Advances

ROYAL SOCIETY OF CHEMISTRY

www.rsc.org/advances

A push-pull organic semiconductor with efficient intramolecular charge transfer for solution-processed small molecule solar cells

Yu Jin Kim,[a] Gi Back Lee,[c] Chan Woo Jeon,[b] Yun-Hi Kim, [b*] Dae Sung Chung [d*] and Chan Eon Park [a*]

[a] POSTECH Organic Electronics Laboratory, Department of Chemical Engineering, Pohang University of Science and Technology, Pohang, 790-784, Republic of Korea

[b] Department of Chemistry & ERI, Gyeongsang National University, Jin-ju, 660-701, Republic of Korea

[c] School of Materials Science & Engineering and Research Institute for Green Energy Convergence Technology (REGET), Gyeongsang National University

[d] School of Chemical Engineering and Material Science Chung-Ang University, Seoul, 156–756, Republic of Korea

*Corresponding Authors:

1. Prof. Chan Eon Park

   POSTECH Organic Electronics Laboratory,

   Department of Chemical Engineering,

   Pohang University of Science and Technology,

   Pohang, 790-784, Republic of Korea

   Email: cep@postech.ac.kr

2. Prof. Yun-Hi Kim

   Department of Chemistry & Research Institute of Natural Science,

   Gyeongsang National University,

   Jin-ju, 660-701, Republic of Korea

   Email: ykim@gnu.ac.kr

3. Prof. Dae Sung Chung

   School of Chemical Engineering and Material Science,

   Chung-Ang University

   Seoul, 156–756, Republic of Korea

   Email: dchung@cau.ac.kr

Correspondence to: Chan Eon Park (E-mail: cep@postech.ac.kr)

Table of Contents

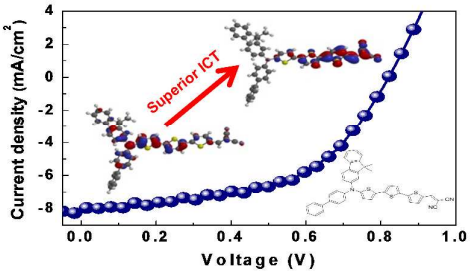

DMF-BP-T-MMN exhibits superior intramolecular charge transfer and excellent solar cell performance with a PCE of 3.40%.

Abstract

A new push-pull organic semiconductor, **DMF-BP-T-MMN**, containing a functionalized amine donor and a methylene malononitrile (MMN) acceptor has been designed and synthesized for use in solution-processable small molecule solar cells. This material exhibits superior intramolecular charge transfer from the functionalized amine group to MMN, which produces an electron-rich MMN group that facilitates electron transfer into the active layer constituent phenyl-C_{71}-butyric acid methyl ester in a solar cell. As a result, **DMF-BP-T-MMN** was found to exhibit excellent p-type semiconductor performance in an optimized organic solar cell: a power conversion efficiency of 3.40% with a high photocurrent density of 8.2 mA/cm^2.

Keywords

Bulk heterojunction solar cell, Organic semiconductor, Small molecule, Intramolecular charge transfer, Power conversion efficiency

Introduction

In recent years, polymer solar cells (PSCs) containing a bulk heterojunction (BHJ) layer have attracted significant attention because they can be fabricated on flexible and light-weight substrates using high-throughput printing techniques and thus have the potential to provide low-cost solar electricity.[1-3] Power conversion efficiencies (PCEs) above 10% have been achieved due to significant improvements in active material design, device structure, device fabrication techniques, morphology control, and characterization methods, etc.[4-6] However, PSCs continue to be affected by the low reproducibility of certain characteristics (for example, the weight-average molecular weight and polydispersity index of the polymer) and the difficulties of purification.[7-8]

Solution-processed small molecule solar cells (SMSCs) have the advantages over PSCs of high purity as well as well-defined structure and molecular weight without batch-to-batch variation, and so have received more and more attention.[9-12] Significant progress in the development of small molecule organic solar cells has recently been made and PCEs of 8–9% have been achieved.[13-14] However, their efficiency is typically lower than that of their polymer counterparts.[15] In order to improve SMSC performance and take full advantage of the properties of small molecules, further systematic research is required. In particular, improvements in active materials, especially in the donor materials, are vital to the production of high PCE SMSCs.

Some structural cores are commonly present in organic semiconductors for SMSCs, such as oligothiophene, bridged dithiophene, benzothiadiazole, squaraine, and diketopyrrolopyrrole, which have been inspired by the low band gap semiconducting materials[16-18] and push-pull molecular structures[19-21] used in nonlinear optics because of their superior optoelectronic properties. A push-pull structure enables efficient intramolecular charge transfer (ICT), which gives the chromophore the required molar absorptivity.[22] In addition, the presence of an

electron donor unit, such as an amine substituted with a fluorene group, can stabilize hole-exciton separation and improve the transport properties of the hole carrier.[23-25]

With this strategy in mind, we have designed and synthesized a new small molecule with a push-pull structure, 2-[{5"-[biphenyl-4-yl-(9,9-dimethyl-9H-fluorene-3yl]-amino}-[2,2',5',2"]terthiophen-5-ylmethylene]-malononitrile (**DMF-BP-T-MMN**). This compound consists of an amine donor, functionalized with fluorene and a bi-phenyl group, and a methylene malononitrile acceptor, which are linked by a terthiophene π-conjugation bridge. As expected, this material was found to exhibit superior ICT to the MMN acceptor through the π-conjugated terthiophene bridge, which produces an electron-rich MMN terminal unit that facilitates electron transfer into $PC_{71}BM$. Small molecule BHJ devices were fabricated by using this compound as the donor and $PC_{71}BM$ as the acceptor. A PCE of 3.40% with a high photocurrent density of 8.2 mA/cm^2 was achieved in an optimized device.

Results and discussion

Synthesis and thermal properties

The synthetic route for **DMF-BP-T-MMN** is shown in Scheme 1. **DMF-BP-T-MMN** was synthesized by performing Buchwald-Hartwig N-arylation, lithiation, and a Suzuki coupling reaction. The chemical structure of the synthesized compound was confirmed with ^{1}H-NMR, ^{13}C-NMR, and mass spectroscopy. This small molecule is readily dissolved in common organic solvents, such as dichlorobenzene, chlorobenzene, chloroform, and toluene, owing to its alkyl-substituted fluorene moiety. The thermal stability of **DMF-BP-T-MMN** was investigated with thermogravimetric analysis (TGA) (Fig. 1a) and differential scanning calorimetry (DSC) (Fig. 1b) at a heating rate of 10°C/min. The TGA profile shows that the onset decomposition temperature (T_d, at 5% weight loss) of **DMF-BP-T-MMN** is 434°C, which indicates that the compound will be fairly stable in long-term photovoltaic

applications.[26] No endothermic or exothermic behavior was found between 25°C and 225°C in the DSC results.

Optical properties

The normalized absorption spectra of the small molecule in chloroform solution and in the thin film state are shown in Fig. 2a, and the corresponding absorption data are listed in Table 1. The **DMF-BP-T-MMN** molecule exhibits strong absorption in the wavelength range 300–800 nm (the visible region) and standard dual absorption profiles due to its ICT band are evident for both the thin film and solution states. The maximum absorption peaks (λ_{max}) of the compound in chloroform are located at 356 and 551 nm. The absorption band at longer wavelengths (500–600 nm) originates from ICT[27] and the absorption band at 350–450 nm is due to π-π* transitions.[28] In the thin film state, the absorption band of **DMF-BP-T-MMN** is stronger and red-shifted compared to that of the solution, which indicates that there are increased π-π* intermolecular interactions in the solid state.[29] The optical band gap (E_g^{opt}) calculated from the film absorption edge is 1.74 eV.

The PL spectra of a spin-cast film of pure **DMF-BP-T-MMN** and of a 1:4 (w/w) blend of the small molecule and $PC_{71}BM$ were examined with the aim of assessing the charge transfer properties of **DMF-BP-T-MMN** (Fig. 2b). The PL spectrum of **DMF-BP-T-MMN** contains a strong PL emission band with a maximum at 644 nm. Upon the addition of $PC_{71}BM$, the emission band is almost completely quenched, which suggests that there is ultrafast and efficient photoinduced charge transfer from the small molecule to PCBM.[30]

Electrochemical properties

In order to investigate the electrochemical properties of the synthesized compound, cyclic voltammetry (CV) measurements were conducted on a **DMF-BP-T-MMN** film on a Pt

electrode at a scan rate of 50 mV/s. The highest occupied molecular orbital (HOMO) level, the lowest unoccupied molecular orbital (LUMO) level, and the electrochemical band gap of **DMF-BP-T-MMN** were calculated from the onset oxidation potential (E_{onset}^{ox}) and the onset reduction potential (E_{onset}^{red}) according to the following equations:

$$E_{HOMO} = -(E_{onset}^{ox} - \text{ferrocene}_{onset}) - 4.8 \text{ eV}$$

$$E_{LUMO} = -(E_{onset}^{red} - \text{ferrocene}_{onset}) - 4.8 \text{ eV}$$

where E_{onset}^{ox} and E_{onset}^{red} were measured relative to Ag/AgCl, and ferrocene_{onset} is the reference onset oxidation potential of ferrocene (0.44 eV).[31]

The CV curve of the small molecule is shown in Fig. 3a and the corresponding electrochemical data are summarized in Table 1. The E_{onset}^{ox} and E_{onset}^{red} of **DMF-BP-T-MMN** were found to be 1.45 and -0.74 V vs. Ag/AgCl respectively, and the corresponding HOMO and LUMO energy levels were estimated to be -5.81 eV and -3.62 eV. These results indicate that **DMF-BP-T-MMN** has the appropriate energy levels to act as a donor in solution-processable organic solar cells with $PC_{71}BM$ as the acceptor (see Fig. 3b).

To investigate the oxidative and reductive properties of **DMF-BP-T-MMN**, its geometry and electronic structure were calculated with density functional theory (DFT). Becke's three parameter gradient corrected functional (B3LYP) with a polarized 6-31 G** basis was used for full geometry optimization. The geometries and the HOMO and LUMO surface plots of the ground-state optimized structure are shown in Fig. 4. The orbital density of the HOMO is located predominantly on the functionalized amine donor, whereas the orbital density of the LUMO has methylene malononitrile (MMN) character. These calculations demonstrate that ICT can occur effectively from the electron-donating amine unit to the MMN acceptor in **DMF-BP-T-MMN** when excited by light energy.[32] The calculated HOMO and LUMO energies of the ground-state optimized geometry of **DMF-BP-T-MMN** are -5.04 eV and -2.96 eV respectively, and the band gap was determined to be 2.08 eV.

Solar cell device performance

Small molecule BHJ solar cells were fabricated with **DMF-BP-T-MMN** as the donor material and $PC_{71}BM$ as the acceptor material by using a conventional solution spin-coating process. The device structure is ITO/PEDOT:PSS/photoactive layer/LiF/Al (see Fig. 5a). Device optimization was conducted by varying the donor *vs*. acceptor weight ratio and the total solution concentration. The current density voltage (*J*-*V*) characteristics under one sun (simulated AM1.5G irradiation at 100 mW cm^{-2}) are shown in Figs. 5b-c and the photovoltaic parameters are presented in Tables 2 and 3. Optimal fabrication conditions were achieved with a **DMF-BP-T-MMN**:$PC_{71}BM$ ratio of 1:4 (w/w); this device was found to exhibit an open-circuit voltage (*V*oc) of 0.79 V, a short-circuit current (*J*sc) of 6.3 mA cm^{-2}, a fill factor (FF) of 43.7%, and a PCE of 2.17% (Fig. 5b). From the photovoltaic measurement, with the decreasing weight ratio of PCBM, J_{SC} and FF showed a gradually reducing trend; a possible explanation for this phenomenon may be from highly phase separated film with quite much aggregation, as shown in the morphology section (see Fig. 6). After optimization with respect to the material concentration, a higher PCE of 2.91% was obtained at a concentration of 20 mg/mL. Therefore, a 1:4 (w/w) blend composition at a solution concentration of 20 mg/mL was used in further device optimization with respect to the use of a processing additive, 1,8-diiodooctane (DIO). As mentioned above, to further improve the photovoltaic performance of **DMF-BP-T-MMN**:$PC_{71}BM$ devices, the DIO additive is used in the active layer. The following DIO volume fractions were used: 0.5, 1, 2 and 4%. The device performance is summarized in Table 3. We found that the presence of the DIO additive leads to an improvement in the device performance. The PCE is elevated to 3.40%, with a *V*oc of 0.78 V, a *J*sc of 8.2 mA cm^{-2}, and a FF of 53.1%, which is the best performance for the **DMF-BP-T-MMN**:$PC_{71}BM$ device processed by with 2 vol% DIO. This improvement in PCE is mainly

due to the improvement in *J*sc (from 7.1 to 8.2 mW cm^{-2}) and changes in properties such as the film morphology and the hole mobility, as discussed below. J_{SC} is strongly dependent on the photo-response (the conversion of input photons to photocurrent).[33] The photo-response of **DMF-BP-T-MMN**:$PC_{71}BM$ processed in the presence of DIO is above 52% at 560 nm, whereas that of **DMF-BP-T-MMN**:$PC_{71}BM$ processed in the absence of this additive is above 46% at 534 nm (Fig. 5d). The higher EQE values of the **DMF-BP-T-MMN**:$PC_{71}BM$ cells processed in the presence of DIO are attributed to the greater conversion of input photons to photocurrent at all absorption wavelengths, as is consistent with the higher circuit current observed.[34]

Film morphology

The performances of solar cell devices are closely associated with the nano-morphologies of their active layers, so we investigated the film morphologies of the **DMF-BP-T-MMN**:$PC_{71}BM$ blend films (1:4, w/w) by performing tapping mode atomic force microscopy (AFM). Figure 7 shows AFM height images of the blend films processed with and without 2 vol% DIO. The blend film in (a) has a relatively homogeneous and flat surface with a root-mean-squared (RMS) roughness of 0.65 nm. In contrast, the spin-coated blend film processed with DIO in (b) has slightly more aggregated domains and a phase-separated surface with a larger RMS roughness of 2.08 nm. The aggregated domains are most likely to have originated from enhancements in the intermolecular interactions of **DMF-BP-T-MMN**.[35] Moreover, the higher roughness of **DMF-BP-T-MMN**:$PC_{71}BM$ processed with 2 vol% DIO means that this film will exhibit reduced internal resistance and more efficient charge separation in SMSCs.[36] A higher surface roughness also leads to increased internal light scattering and enhanced light absorption.[37] All of these characteristics will produce a device with a higher *J*sc value and better efficiency than that exhibited by the **DMF-BP-T-MMN**:$PC_{71}BM$ device processed in

the absence of the additive.

Hole mobility

To investigate space-charge effects, the hole mobilities of the **DMF-BP-T-MMN**:$PC_{71}BM$ blend films were extracted from the space-charge limited current (SCLC) *J-V* characteristics obtained in the dark for hole-only devices. Figure 8 shows the dark-current characteristics of the ITO/PEDOT:PSS/**DMF-BP-T-MMN**:$PC_{71}BM$(1:4)/Au devices prepared with or without DIO as functions of the bias corrected for the built-in voltage determined from the difference between the work functions of Au and PEDOT:PSS-coated ITO. As shown in Fig.8, the average hole mobilities of the blend films processed without and with 2 vol% DIO were found to be 2.17×10^{-6} cm^2/V s and 8.63×10^{-6} cm^2/V s respectively, which is consistent with the J_{SC} values of their solar cells. The hole mobility of the device processed with DIO is higher than that of the device processed without DIO; this difference is closely related to the intermolecular packing interaction as well as to the stability of the charge-exciton separation, which both improve the transport properties of the hole carrier.[38]

Conclusion

We have synthesized a small molecule, **DMF-BP-T-MMN**, which contains a functionalized amine donor and a methylene malononitrile (MMN) acceptor, and investigated its photovoltaic characteristics. This new material exhibits superior intramolecular charge transfer from the functionalized amine group to MMN through a π-conjugated terthiophene bridge, which creates an electron-rich MMN acceptor. This charge transfer process facilitates electron transfer into $PC_{71}BM$, which results in excellent hole-transport properties. SMSCs based on this efficient p-type semiconductor were found to exhibit a PCE of 3.40% after optimization. The results of the molecular engineering approach of this study provide a useful

guide for the development of new materials for solution-processed SMSCs.

Experimental

Materials

All chemical reagents were purchased from Aldrich and TCI. The catalysts used in the coupling reactions were purchased from Umicore. The other materials were of common commercial level and used as received. All solvents were purified prior to use.

Syntheses of materials

Synthesis of N-([1,1'-biphenyl]-4-yl)-9,9-dimethyl-9H-fluoren-2-amine (1)

Compound (1) was prepared according to an established method.[39] Yield: 9.50 g (71.9%). ^{1}H NMR (300 MHz, CD_2Cl_2)[ppm] δ = 7.72-7.60 (m, 6H), 7.51-7.46 (m, 3H), 7.40-7.10 (br, 7H), 6.04 (br, 1H), 1.54 (s, 6H).

Synthesis of N-([1,1'-biphenyl]-4-yl)-N-(9,9-dimethyl-9H-fluoren-2-yl)-[2,2'-bithiophen]-5-amine (2)

N-([1,1'-biphenyl]-4-yl)-9,9-dimethyl-9H-fluoren-2-amine (10.00 g, 27.66 mmol), sodium tert-butoxide (3.19 g, 33.19 mmol), 5-bromo-2,2'-bithiophene (8.14 g, 33.19 mmol), and $Pd_2(dba)_3$ (1.26 g, 1.38 mmol) were dissolved in anhydrous toluene (150 mL) under a nitrogen atmosphere. One portion of P(t-Bu)$_3$ (1.38 mL, 1.38 mmol, 1.0 M in toluene) was added. The solution mixture was slowly heated to reflux, and stirred for 12 h. After cooling, the reaction mixture was extracted with dichloromethane; the combined organic layer was then washed with water and brine, and dried with $MgSO_4$. The residue was chromatographed over silica gel by using dichloromethane/hexane (v/v=1:10) as the eluent. Recrystallization from ethanol afforded a yellow product. Yield: 9.10 g (62.7%). ^{1}H NMR (300 MHz,

CD_2Cl_2)[ppm] δ = 7.72-7.56 (m, 6H), 7.49-7.44 (m, 3H), 7.39-7.28 (m, 6H), 7.24-7.19 (m, 2H), 7.13 (dd, 1H), 7.05 (m, 2H), 6.72 (d, 1H). 1.47 (s, 6H). ^{13}C NMR (500 MHz, $CDCl_3$)[ppm] δ = 155.16, 153.66, 150.50, 147.23, 146.84, 140.56, 138.81, 137.95, 135.63, 135.04, 131.42, 128.78, 127.79, 127.74, 127.02, 126.93, 126.73, 123.79, 122.90, 122.51, 122.37, 122.31, 121.19, 120.65, 119.59, 117.72, 46.96, 27.11. MS (EI) m/z = 525 (M+).

Synthesis of (5'-([1,1'-biphenyl]-4-yl(9,9-dimethyl-9H-fluoren-2-yl)amino)-[2,2'-bithiophen]-5-yl)boronic acid (3)

N-([1,1'-biphenyl]-4-yl)-N-(9,9-dimethyl-9H-fluoren-2-yl)-[2,2'-bithiophen]-5-amine (2) (3.00 g, 5.71 mmol) was dissolved in anhydrous tetrahydrofuran (100 mL) under a nitrogen atmosphere. The solution was cooled to 0°C, then n-BuLi (2.5 M in hexane, 2.51 mL, 6.28 mmol) was added slowly and the reaction mixture was stirred for 2 h. Triisopropyl borate (1.50 g, 7.99 mmol) was added at 0°C. After addition was completed, the reaction mixture was gradually warmed to room temperature and stirred overnight. 2N HCl was added to quench the reaction and then stirred for 1 h. The reaction mixture was extracted with dichloromethane and the combined organic layer was washed with water and brine, then dried with $MgSO_4$. The dichloromethane solution containing the product was reprecipitated in hexane and filtered out. The crude product was transferred to the next reaction step without further purification. Yield: 2.10 g (64.6%).

Synthesis of 2-((5''-([1,1'-biphenyl]-4-yl(9,9-dimethyl-9H-fluoren-2-yl)amino)-[2,2':5',2''-terthiophen]-5-yl)methylene)malononitrile (DMF-BP-T-MMN)

2M K_2CO_3 (6 mL) was added to a solution of (5'-([1,1'-biphenyl]-4-yl(9,9-dimethyl-9H-fluoren-2-yl)amino)-[2,2'-bithiophen]-5-yl)boronic acid (3) (1.66 g, 2.92 mmol) and 2-((5-bromothiophen-2-yl)methylene)malononitrile (0.50 g, 2.09 mmol) in toluene (50 mL). The

mixture was bubbled with nitrogen for 30 min and then $Pd(PPh_3)_4$ was added. The mixture was heated to 100°C for 24 h under a nitrogen atmosphere. The mixture was washed with chloroform and water. After drying over anhydrous $MgSO_4$, the solvent was evaporated. Purification was performed on a silica column with dichloromethane/hexane (v/v=1:5) as the eluent. The dichloromethane solution containing the product was reprecipitated in hexane and filtered out. Yield: 0.98 g (68.5%). ^{1}H NMR (300 MHz, CD_2Cl_2)[ppm] δ = 7.81 (s, 1H), 7.73-7.59 (m, 7H), 7.49-7.45 (m, 3H), 7.41-7.29 (m, 8H), 7.25 (dd, 1H), 7.14 (d, 1H), 7.09 (d, 1H). 6.69 (d, 1H). 1.48 (s, 6H). ^{13}C NMR (500 MHz, $CDCl_3$)[ppm] δ = 155.30, 153.66, 152.91, 149.77, 149.29, 146.81, 146.46, 141.48, 140.38, 140.09, 138.62, 136.37, 135.69, 133.15, 132.49, 128.81, 128.39, 128.23, 127.93, 127.08, 126.93, 126.75, 124.08, 124.02, 123.69, 123.01, 122.93, 122.54, 120.77, 119.69, 119.50, 118.27, 114.36, 113.55, 75.66, 46.99, 31.58, 27.08, 22.64, 14.09. MS (EI) m/z = 683 (M+).

Instruments and measurements

^{1}H-NMR spectra were recorded with a Bruker Avance-300 spectrometer. ^{13}C-NMR spectra were obtained by using a DRX-500 spectrometer. HRMS (EI) spectra were recorded by using a high resolution GC mass spectrometer with LabRAM HR800 UV. Mass (MALDI-TOF/TOF) spectra were obtained on a high resolution 4800 TOF/TOF mass spectrometer with Voyager DE-STR. Thermal analysis (TGA) was performed on a TA Instruments TGA 2100 thermogravimetric analyzer under purified nitrogen at a heating rate of 10°C/min. Differential scanning calorimetry (DSC) was conducted under nitrogen on a TA Instruments 2100 DSC. The sample was heated at 10°C/min from 25 to 225°C. UV-Vis absorption spectra were recorded by using a Cary 5000 UV-vis-near-IR double beam spectrophotometer. Photoluminescence (PL) spectra were obtained with a FP-6500 (JASCO). Cyclic voltammetry (CV) was carried out by using a PowerLab/AD instrument model system in a

0.1 M solution of tetrabutylammonium hexafluorophosphate (Bu_4NPF_6) at a scan rate of 50 mV/s in anhydrous acetonitrile as the supporting electrolyte. A glassy carbon disk (~0.05 cm^2) coated with a thin small molecule film, an Ag/AgCl electrode, and a platinum wire were used as the working electrode, reference electrode, and counter electrode, respectively. Density functional theory (DFT) calculations were carried out at the B3LYP/6-31G* level of theory by using the Spartan 08 computational suite. Atomic force microscopy (AFM) (Multimode Ⅲa, Digital Instruments) was performed in tapping mode to obtain surface images (surface area: 5 × 5 μm^2) of the small molecule:$PC_{71}BM$ blend films processed with and without DIO under ambient conditions.

Fabrication and characterization of the solar cell devices

The devices were fabricated with the conventional structure glass/ITO/PEDOT:PSS/active layer (**DMF-BP-T-MMN**:$PC_{71}BM$)/LiF/Al by using a solution process. The ITO-coated glass substrates were cleaned by washing in detergent, deionized water, acetone, and isopropyl alcohol under ultrasonication for 20 min each and subsequently dried with a nitrogen blower. A thin layer (~40 nm) of PEDOT:PSS (Clevios P VP AI 4083, filtered at 0.45 μm PVDF) was spin-coated at 4000 rpm onto the ITO surface. After baking the substrates at 120°C for 20 min, they were transferred into a nitrogen-filled glovebox. Subsequently, the active layer was spin-coated from donor-acceptor blend solutions with various ratios and total concentrations, and with different volume fraction of the additive 1,8-diiodooctane. Finally, a 0.8 nm LiF layer and a 80 nm Al layer were deposited onto the active layer under high vacuum (2 × 10^{-6} torr). The effective area of each cell was 9 mm^2 as defined by the mask. The current density-voltage (*J-V*) characteristics of the photovoltaic devices were measured under ambient conditions by using a Keithley Model 2400 source-measurement unit. An Oriel xenon lamp (450 W) with an AM1.5G filter was used as the solar simulator. The light intensity was

calibrated to 100 mW/cm^2 by using a calibrated silicon cell with a KG5 filter, which is traced to the National Renewable Energy Laboratory (LREL). The external quantum efficiency (EQE) spectra were obtained by using a photomodulation spectroscopic set-up (model Merlin, Oriel), a calibrated Si UV detector, and a SR570 low noise current amplifier.

Hole mobility measurements

Hole-only devices were fabricated with the configuration ITO/PEDOT:PSS/**DMF-BP-T-MMN**:$PC_{71}BM$/Au. The Au layers was deposited at a low speed (1 /s) to prevent the penetration of Au atoms into the active layers. The active layers were spin-coated with or without DIO (2 vol%). The mobilities were extracted by fitting the current-voltage curves with the Mott-Gurney relationship (space charge limited current):

$$J = \frac{9}{8}\varepsilon_0\varepsilon_r\mu_h\frac{V^2}{L^3}$$

where J is the current density, L is the film thickness of the active layer, μ_h is the hole mobility, ε_r is the relative dielectric constant of the transport medium, ε_0 is the permittivity of free space, V is the internal voltage of the device, and $V = V_{appl} - V_r - V_{bi}$. V_{appl} is the applied voltage to the device, V_r is the voltage drop due to contact resistance and series resistance across the electrodes, and V_{bi} is the built-in voltage due to the difference between the work functions of the two electrodes. V_{bi} can be determined from the transition between the ohmic region and the SCLC region.

Acknowledgements

This study was supported by a grant from the National Research Foundation of Korea (NRF), funded by the Korean Government (MSIP NRF-2014R1A2A1A05004993), and by the New & Renewable Energy Technology Development Program of KETEP (20113020010070). This

research was also supported by the Chung-Ang University Research Scholarship Grants in 2013.

Notes and references

1 S. Gunes, H. Neugebauer, N. S. Sariciftci, *Chem. Rev*., 2007, **107**, 1324.

2 Y. -J. Cheng, S. -H. Yang, C. -S. Hsu, *Chem. Rev*., 2009, **109**, 5868.

3 J. Jo , A. Pron, P. Berrouard, W. L. Leong, J. D. Yuen, J. S. Moon, M. Leclerc, and A. J. Heeger, *Adv. Energy Mater*., 2012, **2**, 1397.

4 G. Li, R. Zhu, and Y. Yang, *Nat. Photo*., 2012, **6**, 153.

5 H. Zhou, L. Yang, and W. You, Macromolecules, 2012, **45**, 607.

6 L. –M. Chen, Z. Hong, G. Li, and Y. Yang, *Adv. Mater*., 2009, **21**, 1434.

7 B. Walker, C. Kim, and T. –Q. Nguyen, *Chem. Mater*., 2011, **23**, 470.

8 O. P. Lee, A. T. Yiu, P. M. Beaujuge, C. H. Woo, T. W. Holcombe, J. E. Millstone, J. D. Douglas, M. S. Chen and J. M. J. Fréchet, *Adv. Mater*., 2011, **23,** 5359.

9 Y. Sun, G. C. Welch, W. L. Leong, C. J. Takacs, G. C. Bazan, and A. J. Heeger, *Nat. Mater*., 2012, **11**, 44.

10 J. A. Love, C. M. Proctor, J. Liu, C. J. Takacs, A. Sharenko, T. S. van der Poll, A. J. Heeger, G. C. Bazan, and T. –Q. Nguyen, *Adv. Funct. Mater*., 2013, **23**, 4990.

11 Y. Liu, L. Ma, Y. Li, Y. Liu, D. Zhu, and X. Zhan, *Adv. Energy. Mater*., 2013, **3**, 1166.

12 H. –Y. Lin, W. –C. Huang, Y. –C. Chen, H. –H. Chou, C. –Y. Hsu, J. T. Lin and H. –W. Lin, *Chem. Commun*., 2012, **48**, 8913.

13 J. Zhou, Y. Zuo, X. Wan, G. Long, Q. Zhang, W. Ni, Y. Liu, Z. Li, G. He, C. Li, B. Kan, M. Li, and Y. Chen, *J. Am. Chem. Soc.*, 2013, **135**, 8484.

14 Y. Liu, C. –C. Chen, Z. Hong, J. Gao, Y. (Michael) Yang, H. Zhou, L. Dou, G. Li, and Y. Yang, *Sci. Rep*., 2013, **3**, 3356.

15 Y. Chen, X. Wan, and G. Long, *Acc. Chem. Res*., 2013, **46**, 2645.

16 A. Mishra, and P. Bäuerle, *Angew. Chem. Int. Ed*., 2012, **51**, 2020.

17 J. Roncali, P. Leriche, and P. Blanchard, *Adv. Mater*., 2014, DOI: 10.1002/adma.201305999

18 H. Wang, F. Liu, L. Bu, J. Gao, C. Wang, W. Wei, and T. P. Russell, *Adv. Mater*., 2013, **25**, 6519.

19 J. Zhang, L. Yang, M. Zhang, and P. Wang, *RSC Adv*., 2013, **3**, 6030.

20 J. Liu, Y. Sun, P. Moonsin, M. Kuik, C. M. Proctor, J. Lin, B. B. Hsu, V. Promarak, A. J. Heeger, and T. –Q. Nguyen, *Adv. Mater*., 2013, **25**, 5898.

21 A. Sutter, P. Retailleau, W. –C. Haung, H. –W. Lin and R. Ziessel, *New J. Chem*., 2014, **38**, 1701.

22 T. M. Clarke, and J. R. Durrant, *Chem. Rev*., 2010, **110**, 6736.

23 S. –C. Lo, and P. L. Burn, *Chem. Rev*., 2007, **107**, 1097.

24 J. H. Delcamp, A. Yella, T. W. Holcombe, M. K. Nazeeruddin, and M. Grätzel, *Angew. Chem. Int. Ed*., 2013, **52**, 376.

25 H. –W. Lin, J. –H. Chang, W. –C. Huang, Y. –T. Lin, L. –Y. Lin, F. Lin, K. –T. Wong, H. –F. Wang, R. –M. Ho and H. –F. Meng, *J. Mater. Chem. A*., 2014, **2**, 3709.

26 G. He, Z. Li, X. Wan, J. Zhou, G. Long, S. Zhang, M. Zhang, and Y. Chen, *J. Mater. Chem. A*., 2013, **1**, 1801.

27 Y. Li, K. Yao, H. –L. Yip, F. –Z. Ding, Y. –X. Xu, X. Li, Y. Chen, and A. K. –Y. Jen, *Adv. Funct. Mater.* 2014, DOI: 10.1002/adfm.201303953

28 Y. J. Kim, K. H. Park, J. –j. Ha, D. S. Chung, Y. –H. Kim, and C. E. Park, Phys. *Chem. Chem. Phys*., 2014, DOI: 10.1039/c4cp00077c.

29 P. Dutta, W. Yang, S. H. Eom, W. –H. Lee, I. N. Kang, and S. –H. Lee, *Chem. Commun*., 2012, **48**, 573.

30 T. Ameri, P. Khoram, J. Min, and C. J. Brabec, *Adv. Mater*., 2013, **25,** 4245.

31 L. Fu, W. Fu, P. Cheng, Z. Xie, C. Fan, M. Shi, J. Ling, J. Hou, X. Zhan and H., Chen, *J. Mater. Chem. C*, 2014, DOI: 10.1039/c3ta13534a.

32 K. DO, C. Kim, K. Song, S. J. Yin, J. K. Lee, and J. Ko, *Sol. Energy Mater. & Sol. Cells*, 2013, **115**, 52.

33 L. Dou, J. You, J. Yang, C. –C. Chen, Y. He, S. Murase, T. Moriarty, K. Emery, G. Li, and Y. Yang, *Nat. Photon*., 2012, **6**, 180.

34 T. S. van der Poll, J. A. Love, T. –Q. Nguyen, and G. C. Bazan, *Adv. Mater*., 2012, **24**, 3646.

35 Q. Shi, P. Cheng, Y. Li, X. Zhan, *Adv. Ener. Mater*., 2012, **2**, 63.

36 Q. Peng, X. Liu, Y. Qin, D. Zhou, and J. Xu, *J. Polym. Sci. Part A: Polym. Chem.*, 2011, **49**, 4458.

37 J. D. Zimmerman, X. Xiao, C. K. Renshaw, S. Wang, V. V. Diev, M. E. Thompson, S. R. Forrest, *Nano. Lett*. 2012, **12**, 4366.

38 R. Shivanna, S. Shoaee, S. Dimitrov, S. K. Kandappa, S. Rajaram, J. R. Durrant, and K. S. Narayan, *Energy Environ. Sci*., 2014, **7**, 435.

39 S. –H. Hwang, Y. K. Kim, Y. Kwak, C. –H. Lee, J. Lee, S. Kim, *Synth. Met*., 2009, 159, 2578.

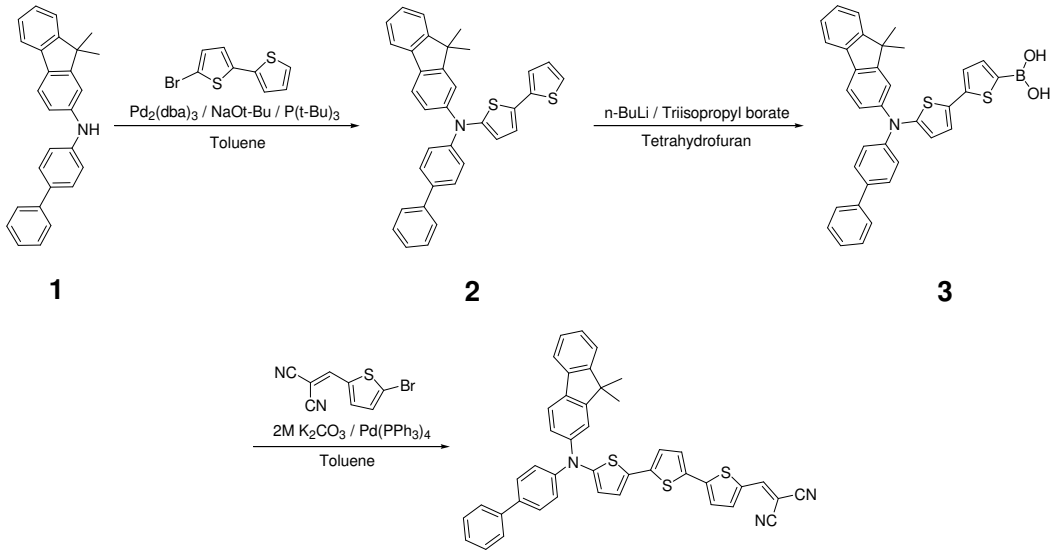

Scheme 1. Synthetic route for **DMF-BP-T-MMN**.

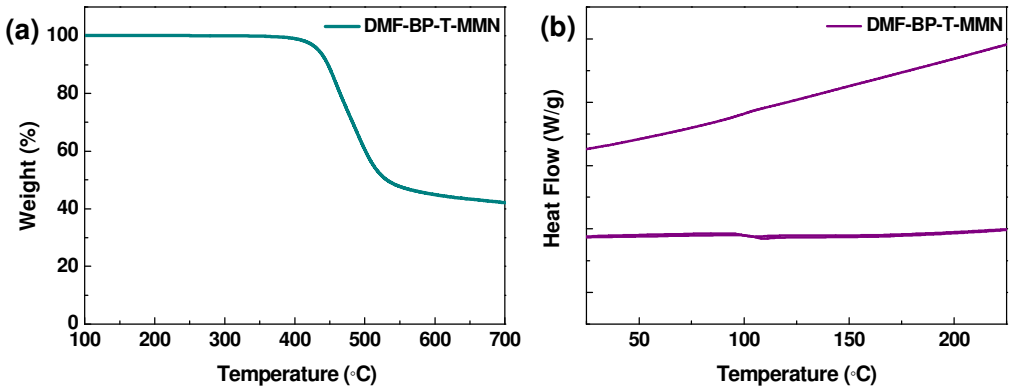

Fig. 1. TGA plot for **DMF-BP-T-MMN** (a) and DSC curves for **DMF-BP-T-MMN** (b) recorded at a heating rate of 10°C/min.

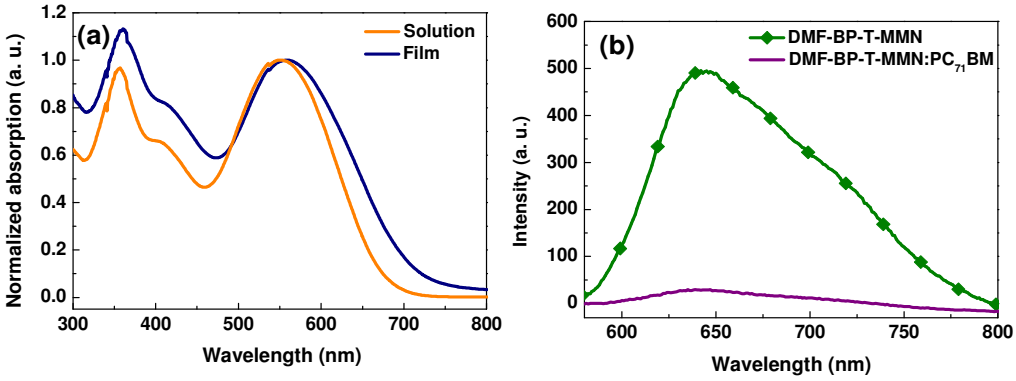

Fig. 2. (a) Normalized UV-vis absorption spectra of **DMF-BP-T-MMN** in chloroform and in the thin film state at room temperature; (b) Photoluminescence spectra of **DMF-BP-T-MMN** and a **DMF-BP-T-MMN**:$PC_{71}BM$ blend film.

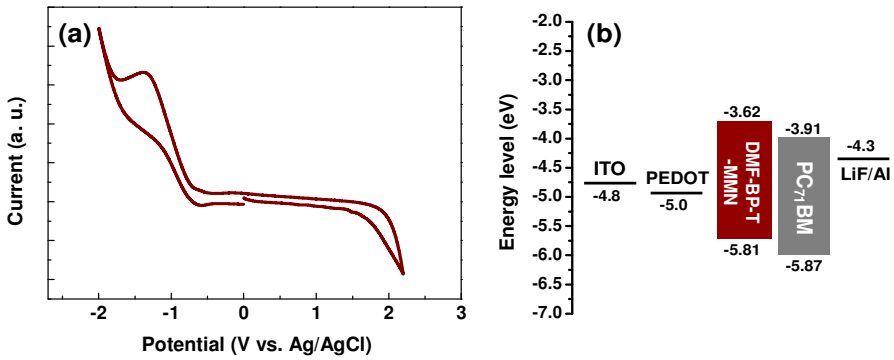

Fig. 3. (a) Cyclic voltammogram of **DMF-BP-T-MMN**, and (b) energy level diagram for the component materials of the devices.

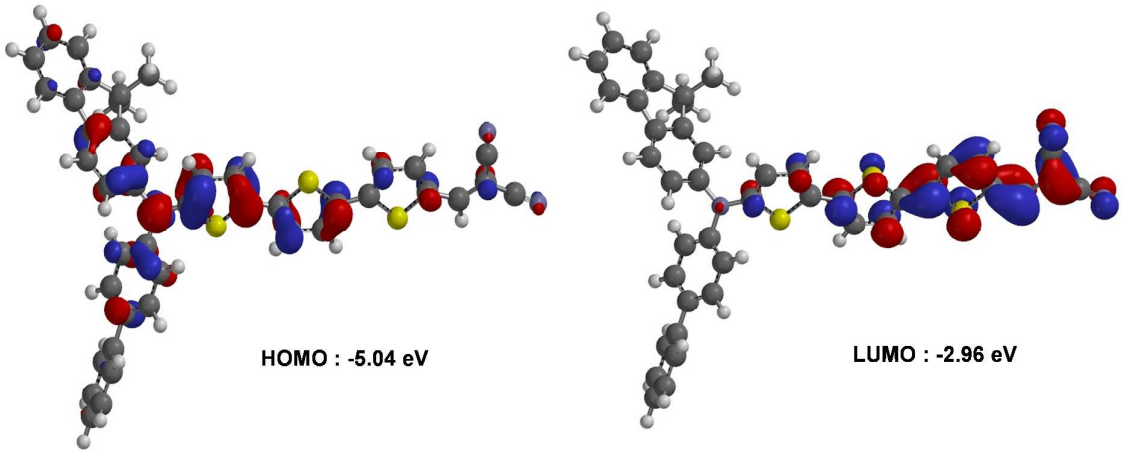

Fig. 4. Isodensity surface plots of **DMF-BP-T-MMN** calculated with DFT.

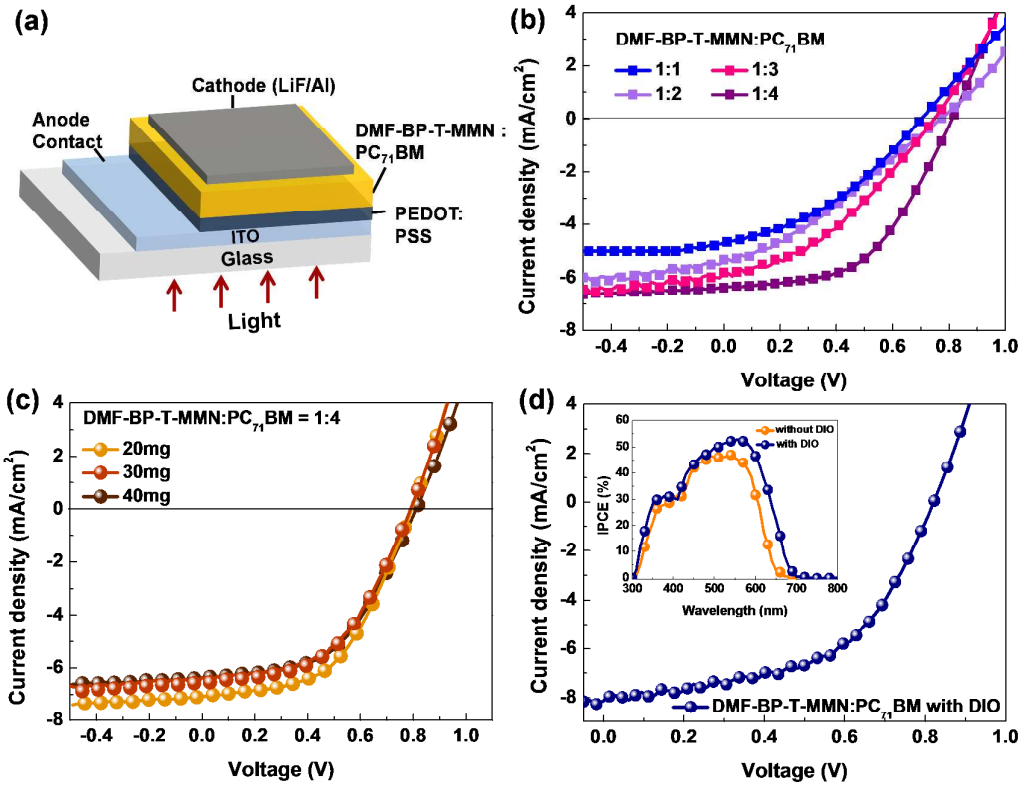

Fig. 5. Schematic diagram of the photovoltaic cell. (b), (c) *J-V* curves for various **DMF-BP-T-MMN**:$PC_{71}BM$ blend ratios and solution concentrations respectively. (d) *J-V* curve obtained from the best-performing device processed in the presence of 2 vol% DIO. The inset shows the IPCE spectra of the devices processed with and without the DIO additive.

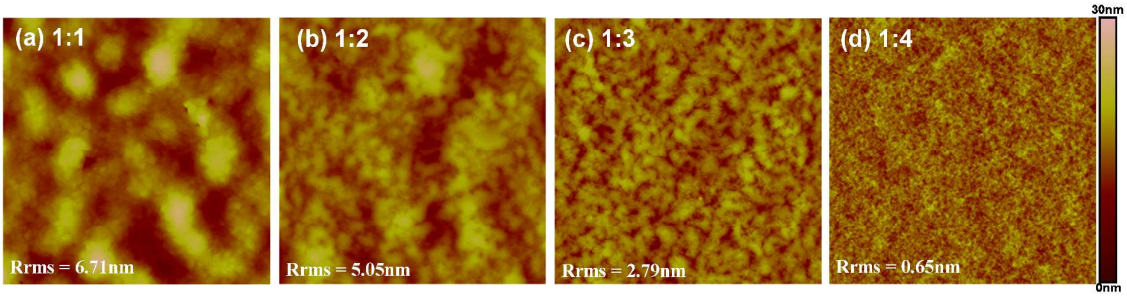

Fig. 6. AFM height images for **DMF-BP-T-MMN**:$PC_{71}BM$ blend films with different weight ratios spin coated from chloroform: (a) 1:1, (b) 1:2, (c) 1:3, and (d) 1:4.

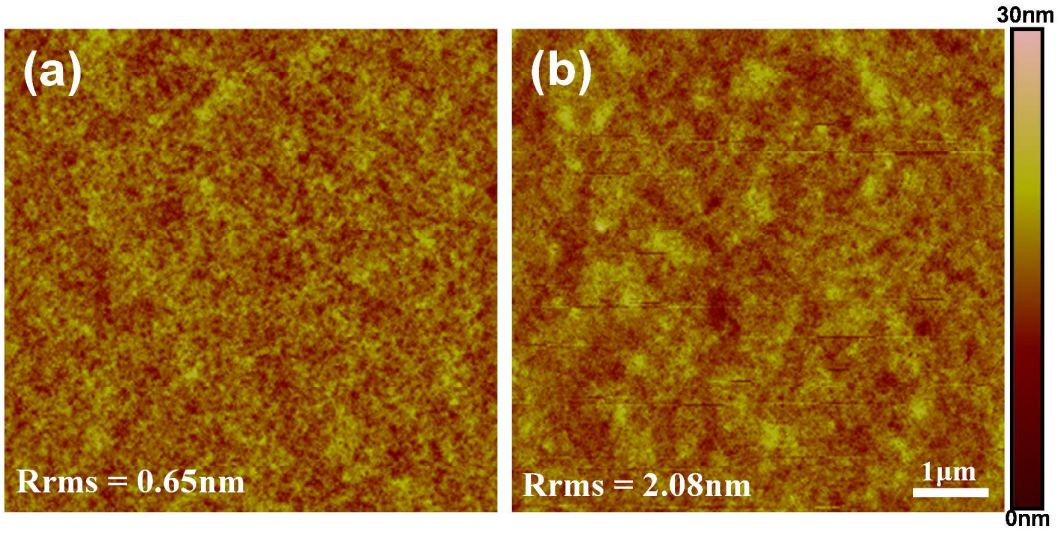

Fig. 7. Tapping-mode AFM surface topographies of **DMF-BP-T-MMN**:$PC_{71}BM$ (1:4) films processed without (a) and with (b) 2 vol% DIO.

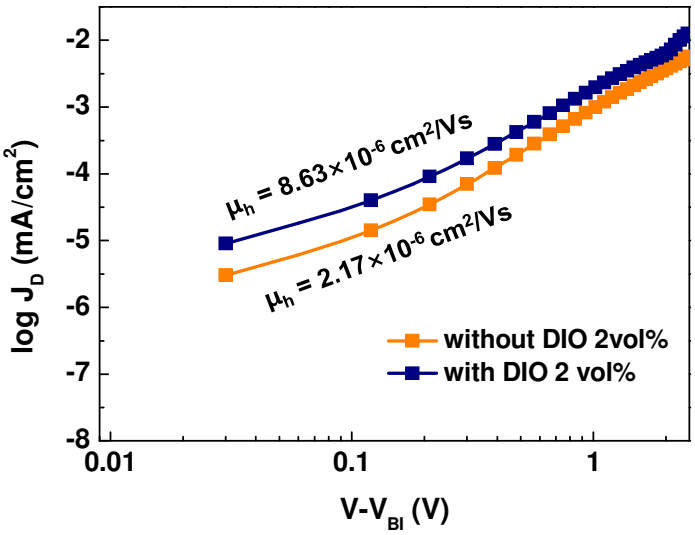

Fig. 8. Hole mobilities of **DMF-BP-T-MMN**:$PC_{71}BM$ cast from bare solvent and from solvent containing 2 vol% DIO.

Table 1. Optical and electrochemical characteristics of **DMF-BP-T-MMN**.

Small Molecule	λ_{max} (nm) solution	λ_{max} (nm) film	λ_{onset} (nm) film	E_g^{opt} (eV)[a]	E_{onset}^{ox} (eV)	E_{onset}^{red} (eV)	E_{HOMO} (eV)	E_{LUMO} (eV)
DMF-BP-T-MMN	356, 551	360, 560	713	1.74	1.45	-0.74	-5.81	-3.62

[a] Estimated from the absorption edge of the film ($E_g^{opt} = 1240/\lambda_{onset}$ eV).

Table 2. Summary of the parameters of the devices containing various **DMF-BP-T-MMN**:$PC_{71}BM$ compositions blended in chloroform.

Small molecule : PCBM	Blend ratios	*V*oc (V)	*J*sc (mA / cm^2)	FF (%)	PCE (%)
DMF-BP-T-MMN :$PC_{71}BM$	1:1	0.74	4.7	28.4	0.98
	1:2	0.77	5.3	31.8	1.33
	1:3	0.75	5.9	39.5	1.74
	1:4	0.79	6.3	43.7	2.17

Table 3. Photovoltaic data for the **DMF-BP-T-MMN**:$PC_{71}BM$ (1:4 w/w) devices for various total concentrations.

Small molecule : PCBM	Total concentration (mg/mL)	*V*oc (V)	*J*sc (mA / cm^2)	FF (%)	PCE (%)
DMF-BP-T-MMN :$PC_{71}BM$	20	0.79	7.1	52.0	2.91
	30	0.78	6.7	50.8	2.65
	40	0.79	6.3	43.7	2.17

Table 4. Device performance of various amounts of DIO additive in the **DMF-BP-T-MMN**:$PC_{71}BM$ (1:4 w/w) cell.

Small molecule : PCBM	DIO additive [vol%]	*V*oc (V)	*J*sc (mA / cm^2)	FF (%)	PCE (%)
DMF-BP-T-MMN :$PC_{71}BM$	0.5	0.70	3.7	38.2	0.98
	1	0.76	6.1	50.9	2.36
	2	0.78	8.2	53.1	3.40
	4	0.72	4.4	42.8	1.35